Eur. Phys. J. D **40**, 147–156 (2006)
DOI: 10.1140/epjd/e2006-00141-0

THE EUROPEAN PHYSICAL JOURNAL D

Controllable shape-matched propagation of two signal beams in a double-Λ atomic ensemble

Zhuan Li[1], Li-Ping Deng[1], Li-Sen Xu[1], and Kaige Wang[2,1,3,a]

[1] Department of Physics, Applied Optics Beijing Area Major Laboratory, Beijing Normal University, Beijing 100875, P.R. China
[2] CCAST (World Laboratory), P.O. Box 8730, Beijing 100080, P.R. China
[3] The Abdus Salam International Centre for Theoretical Physics, 34014 Trieste, Italy

Received 14 October 2005 / Received in final form 10 March 2006
Published online 21 June 2006 –

Abstract. We study a four-level double-Λ atomic ensemble interacting with two time-dependent signal fields and two stationary control fields. Though, in each Λ channel, a pair of signal and control fields couple resonantly with the two lower levels of atoms, the occurrences of electromagnetically induced transparency (EIT) is affected by the coherence of the four fields. In the discussion of atomic susceptibilities, we show that the quantum coherence between the two lower levels can be either formed or released according to the phase matching of the four fields. We analyze the propagation equation of the two signal fields, and find two characteristic solutions: the stationary transmission wave and the transient decay wave. The former corresponds to a correlated EIT effect in which two signal pulses are shape-matched. The latter is an opposite effect to the correlated EIT in which two pulses quench simultaneously, thus named as the correlated two-signal absorption (CTSA). We propose the CTSA condition in correspondence with the EIT condition. The numerical simulation shows that the double-Λ configuration is capable of manipulating synchronous optical signals and thus provides multiplicity and versatility in quantum information process.

PACS. 42.50.Gy Effects of atomic coherence on propagation, absorption, and amplification of light; electromagnetically induced transparency and absorption – 42.50.Hz Strong-field excitation of optical transitions in quantum systems; multiphoton processes; dynamic Stark shift – 42.65.-k Nonlinear optics

1 Introduction

Electromagnetically induced transparency (EIT) has drawn much attention in recent years. The EIT system consists of atoms with a three-level Λ configuration, interacting with both a signal (or probe) and a control (or driving) field [1]. Since quantum coherence occurs in the EIT interaction, the signal or quantum state can be transferred between the atoms and the field [2–9]. The scheme is the basis of quantum memory, which is one of the key devices in quantum information technique. The EIT effect can also occur in a four-level double-Λ configuration interacting with two couples of signal and control fields [10–21]. References [10–12] show that, in the double-Λ configuration, two shape-matched probe pulses interacting with one Λ channel can losslessly propagate while two identical strong pulses drive the other Λ channel. Theoretical analysis pointed out that the EIT effect in the double-Λ configuration requires a Rabi-frequency matching of four fields, and it has been demonstrated in experiments [11,13]. However, the ultraslow propagation and the storage mechanism of optical pulse in the standard EIT interaction can also be applied to the double-Λ configuration, where two probe pulses can be stored and released simultaneously [16–21].

In a double-Λ configuration, the two Λ subsystems share a common dark state so that the quantum interference exists not only in each Λ channel, but also between the two Λ channels. This feature renders the four-level scheme flexible and versatile in practical applications. In this paper, we study the atomic susceptibilities, the propagation solutions and the manipulation of shape-matched signals in a double-Λ atomic system. We formulate the atomic susceptibilities, and find that the quantum coherence of the two lower levels is related to the phase matching of the four fields. In analytical solution of the propagation equation, the two characteristic solutions, the stationary transmission wave and the transient decay wave, are obtained. The former corresponds to the correlated EIT effect in which the two pulses propagate synchronously. The latter reflects an opposite effect to the EIT, the correlated two-signal absorption (CTSA), in

[a] e-mail: wangkg@bnu.edu.cn

which the two pulses decay and quench simultaneously. The phase matching of the four fields dominates the two characteristic solutions. In the EIT case, however, the two transmitted signals are synchronously modulated in the quantum correlation between the two Λ channels. In the double-Λ configuration, the dark state polariton-wave, consisting of both the two signal fields and the atomic coherence of two lower levels, propagates losslessly [17,19]. Therefore, by adiabatically changing the two control fields, the signals can be transferred not only between the fields and the atomic medium but also between the two fields. Our numerical simulations show a variety of schemes for manipulating synchronous optical signals, such as signal copy (generation of optical twin signals), signal amplification, and signal transfer among the two fields and the atomic medium.

2 Model and equations of motion

We consider a model consisting of atoms with a double-Λ configuration interacting with four laser fields, as depicted in Figure 1, where Ω_u and ω_u $(u = 1s, 2s, 1c, 2c)$ are designated as the Rabi frequency and the carrier frequency of the field, respectively. Here we assume two detuning schemes. In detuning scheme I shown in Figure 1a, the two weak signal fields Ω_{1s} and Ω_{2s} couple the atomic transitions $|b\rangle - |a\rangle$ and $|b\rangle - |d\rangle$, respectively, with the same detuning $\Delta = \omega_{ab} - \omega_{1s} = \omega_{db} - \omega_{2s}$, while the two strong control fields Ω_{1c} and Ω_{2c} are resonant with the transitions $|c\rangle - |a\rangle$ and $|c\rangle - |d\rangle$ (i.e. $\omega_{1c} = \omega_{ac}$ and $\omega_{2c} = \omega_{dc}$), respectively, where ω_{ab}, ω_{ac}, ω_{db}, and ω_{dc} stand for the atomic transition frequencies. In detuning scheme II shown in Figure 1b, a pair of fields in one Λ channel, Ω_{1s} and Ω_{1c}, are resonant with the corresponding atomic transitions (i.e. $\omega_{1s} = \omega_{ab}$ and $\omega_{1c} = \omega_{ac}$), while the pair of fields in the other Λ channel, Ω_{2s} and Ω_{2c}, are detuned from the atomic transitions with the same detuning $\Delta = \omega_{db} - \omega_{2s} = \omega_{dc} - \omega_{2c}$. Accordingly, the Raman transitions occur in both Λ channels. However, the dipole transitions $|b\rangle - |c\rangle$ and $|a\rangle - |d\rangle$ are forbidden.

The Hamiltonian of the system is $H = H_0 + H_I$, in which the free Hamiltonians for the two detuning schemes are defined as

$$H_0 = \hbar \sum_{j=1}^{N} [(\omega_a - \Delta) |a_j\rangle \langle a_j| + (\omega_d - \Delta) |d_j\rangle \langle d_j| + (\omega_c - \Delta) |c_j\rangle \langle c_j| + \omega_b |b_j\rangle \langle b_j|], \quad \text{for detuning scheme I,} \tag{1a}$$

$$H_0 = \hbar \sum_{j=1}^{N} [\omega_a |a_j\rangle \langle a_j| + (\omega_d - \Delta) |d_j\rangle \langle d_j| + \omega_c |c_j\rangle \langle c_j| + \omega_b |b_j\rangle \langle b_j|], \quad \text{for detuning scheme II,} \tag{1b}$$

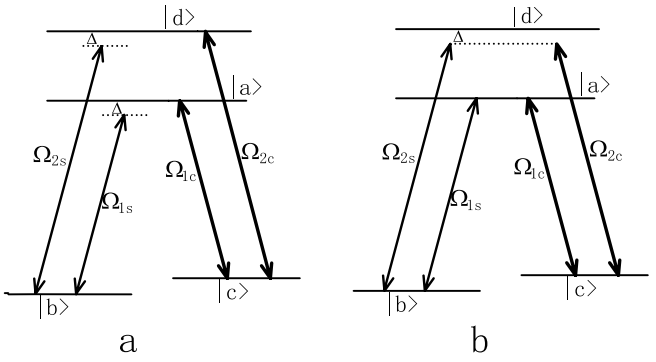

Fig. 1. Four-level Double-Λ atomic system; (a) detuning scheme I and (b) detuning scheme II.

where N is the total number of atoms. In the interaction picture, the interaction Hamiltonian can be written as

$$\begin{aligned} H_I = H_\Delta - \frac{\hbar}{2} \sum_{j=1}^{N} \{ & \Omega_{1s} |a_j\rangle \langle b_j| \exp[ik_{1s} z_j] \\ & + \Omega_{2s} |d_j\rangle \langle b_j| \exp[ik_{2s} z_j] \\ & + \Omega_{1c} |a_j\rangle \langle c_j| \exp[ik_{1c} z_j] \\ & + \Omega_{2c} |d_j\rangle \langle c_j| \exp[ik_{2c} z_j] + H.c. \}, \end{aligned} \tag{2}$$

where z_j is the position of the jth atom. The wavevectors of the fields are $k_u = \omega_u / c$ $(u = 1s, 2s, 1c, 2c)$, and the relation $k_{1c} - k_{2c} = k_{1s} - k_{2s}$ is valid for both detuning schemes. H_Δ is the term related to detuning,

$$H_\Delta = \hbar \Delta \sum_{j=1}^{N} (|a_j\rangle \langle a_j| + |d_j\rangle \langle d_j| + |c_j\rangle \langle c_j|), \quad \text{for detuning scheme I,} \tag{3a}$$

$$H_\Delta = \hbar \Delta \sum_{j=1}^{N} |d_j\rangle \langle d_j|, \quad \text{for detuning scheme II.} \tag{3b}$$

For detuning scheme I, we obtain the density-matrix equations for the single atom at the position z

$$\frac{\partial \rho_{ca}}{\partial t} = -\frac{1}{2}(\Gamma_b^a + \Gamma_c^a)\rho_{ca} - \frac{i}{2}[\Omega_{1s}^* \rho_{cb} + \Omega_{1c}^* (\rho_{cc} - \rho_{aa}) - \Omega_{2c}^* \rho_{da}], \tag{4a}$$

$$\frac{\partial \rho_{db}}{\partial t} = -\left[\frac{1}{2}(\Gamma_b^d + \Gamma_c^d) + i\Delta\right] \rho_{db} - \frac{i}{2}[\Omega_{1s} \rho_{da} + \Omega_{2s} (\rho_{dd} - \rho_{bb}) - \Omega_{2c} \rho_{cb}], \tag{4b}$$

$$\frac{\partial \rho_{aa}}{\partial t} = -(\Gamma_b^a + \Gamma_c^a)\rho_{aa} - \frac{i}{2}[\Omega_{1s}^* \rho_{ab} - \Omega_{1s} \rho_{ba} + \Omega_{1c}^* \rho_{ac} - \Omega_{1c} \rho_{ca}], \tag{4c}$$

$$\frac{\partial \rho_{bb}}{\partial t} = \Gamma_b^a \rho_{aa} + \Gamma_b^d \rho_{dd} - \frac{i}{2}[\Omega_{1s} \rho_{ba} - \Omega_{1s}^* \rho_{ab} + \Omega_{2s} \rho_{bd} - \Omega_{2s}^* \rho_{db}], \tag{4d}$$

$$\frac{\partial\rho_{cc}}{\partial t} = \Gamma_c^a\rho_{aa} + \Gamma_c^d\rho_{dd} - \frac{i}{2}[\Omega_{1c}\rho_{ca} - \Omega_{1c}^*\rho_{ac} + \Omega_{2c}\rho_{cd} - \Omega_{2c}^*\rho_{dc}], \quad (4e)$$

$$\frac{\partial\rho_{dd}}{\partial t} = -(\Gamma_b^d + \Gamma_c^d)\rho_{dd} - \frac{i}{2}[\Omega_{2s}^*\rho_{db} - \Omega_{2s}\rho_{bd} - \Omega_{2c}\rho_{cd} + \Omega_{2c}^*\rho_{dc}], \quad (4f)$$

and

$$\frac{\partial\rho_{ab}}{\partial t} = -\left[\frac{1}{2}(\Gamma_b^a + \Gamma_c^a) + i\Delta\right]\rho_{ab} - \frac{i}{2}\{\Omega_{1s}(\rho_{aa} - \rho_{bb}) + \Omega_{2s}\rho_{ad} - \Omega_{1c}\rho_{cb}\}, \quad (5a)$$

$$\frac{\partial\rho_{cb}}{\partial t} = -i\Delta\rho_{cb} - \frac{i}{2}\{\Omega_{1s}\rho_{ca} + \Omega_{2s}\rho_{cd} - \Omega_{1c}^*\rho_{ab} - \Omega_{2c}^*\rho_{db}\}, \quad (5b)$$

$$\frac{\partial\rho_{cd}}{\partial t} = -\frac{1}{2}\left(\Gamma_b^d + \Gamma_c^d\right)\rho_{cd} - \frac{i}{2}\{\Omega_{2s}^*\rho_{cb} + \Omega_{2c}^*(\rho_{cc} - \rho_{dd}) - \Omega_{1c}^*\rho_{ad}\}, \quad (5c)$$

$$\frac{\partial\rho_{da}}{\partial t} = -\frac{1}{2}\left(\Gamma_b^a + \Gamma_c^a + \Gamma_b^d + \Gamma_c^d\right)\rho_{da} - \frac{i}{2}\{\Omega_{1s}^*\rho_{db} - \Omega_{2s}\rho_{ba} + \Omega_{1c}^*\rho_{dc} - \Omega_{2c}\rho_{ca}\}, \quad (5d)$$

where Γ_b^a and Γ_c^a (Γ_b^d and Γ_c^d) are the decay rates from the upper level $|a\rangle$ ($|d\rangle$) to the two lower levels $|b\rangle$ and $|c\rangle$, respectively. As for detuning scheme II, equations (5) are replaced by

$$\frac{\partial\rho_{ab}}{\partial t} = -\frac{1}{2}(\Gamma_b^a + \Gamma_c^a)\rho_{ab} - \frac{i}{2}\left[\Omega_{1s}(\rho_{aa} - \rho_{bb}) + \Omega_{2s}\rho_{ad} - \Omega_{1c}\rho_{cb}\right], \quad (6a)$$

$$\frac{\partial\rho_{cb}}{\partial t} = -\frac{i}{2}\left[\Omega_{1s}\rho_{ca} + \Omega_{2s}\rho_{cd} - \Omega_{1c}^*\rho_{ab} - \Omega_{2c}^*\rho_{db}\right], \quad (6b)$$

$$\frac{\partial\rho_{cd}}{\partial t} = -\left[\frac{1}{2}(\Gamma_b^d + \Gamma_c^d) - i\Delta\right]\rho_{cd} - \frac{i}{2}\left[\Omega_{2s}^*\rho_{cb} + \Omega_{2c}^*(\rho_{cc} - \rho_{dd}) - \Omega_{1c}^*\rho_{ad}\right], \quad (6c)$$

$$\frac{\partial\rho_{da}}{\partial t} = -\left[\frac{1}{2}(\Gamma_b^a + \Gamma_c^a + \Gamma_b^d + \Gamma_c^d) + i\Delta\right]\rho_{da} - \frac{i}{2}\left[\Omega_{1s}^*\rho_{db} - \Omega_{2s}\rho_{ba} + \Omega_{1c}^*\rho_{dc} - \Omega_{2c}\rho_{ca}\right]. \quad (6d)$$

In the slowly varying envelope approximation [22,23], the propagation equations of the two signal fields are written as

$$c\frac{\partial\Omega_{1s}}{\partial z} + \frac{\partial\Omega_{1s}}{\partial t} = \frac{i}{2}g_1^2N\rho_{ab}, \quad (7a)$$

$$c\frac{\partial\Omega_{2s}}{\partial z} + \frac{\partial\Omega_{2s}}{\partial t} = \frac{i}{2}g_2^2N\rho_{db}, \quad (7b)$$

where c is the light velocity in vacuum, and $g_1 = \wp_{ba}\sqrt{2\omega_{1s}/(\varepsilon_0V\hbar)}$, $g_2 = \wp_{bd}\sqrt{2\omega_{2s}/(\varepsilon_0V\hbar)}$ are the coupling coefficients. $\wp_{ba}$ and $\wp_{bd}$ are the dipole moments, and V is the volume of the medium, and ε_0, the vacuum electric permittivity. In order to minimize the parameters of the model, we assume balanced decay and coupling, i.e. $\Gamma_b^a = \Gamma_c^a = \Gamma_b^d = \Gamma_c^d = \gamma$ and $g_1 = g_2 = g$. However, the two control fields are set to be plane-waves.

3 Atomic susceptibilities

We formulate the atomic susceptibilities for the two weak signal fields. In the limit of strong control fields, most atoms are populated at the ground state $|b\rangle$, that is $\rho_{bb} \approx 1$ and $\rho_{aa} \approx \rho_{cc} \approx \rho_{dd} \approx 0$. For detuning scheme I, we obtain the stationary equations

$$(\gamma + i\Delta)\rho_{ab} = (i/2)(\Omega_{1s} + \Omega_{1c}\rho_{cb}), \quad (8a)$$

$$(\gamma + i\Delta)\rho_{db} = (i/2)(\Omega_{2s} + \Omega_{2c}\rho_{cb}), \quad (8b)$$

$$\Delta\rho_{cb} = (1/2)(\Omega_{1c}^*\rho_{ab} + \Omega_{2c}^*\rho_{db}). \quad (8c)$$

The atomic coherence can be solved as

$$\rho_{ab} = \frac{[4(\Delta - i\gamma)\Delta - |\Omega_{2c}|^2]\Omega_{1s} + \Omega_{1c}\Omega_{2c}^*\Omega_{2s}}{2(\Delta - i\gamma)(4\Delta^2 - |\Omega_c|^2 - i4\Delta\gamma)}, \quad (9a)$$

$$\rho_{db} = \frac{[4(\Delta - i\gamma)\Delta - |\Omega_{1c}|^2]\Omega_{2s} + \Omega_{1c}^*\Omega_{2c}\Omega_{1s}}{2(\Delta - i\gamma)(4\Delta^2 - |\Omega_c|^2 - i4\Delta\gamma)}, \quad (9b)$$

where the total intensity of the control fields is designated by $|\Omega_c|^2 \equiv |\Omega_{1c}|^2 + |\Omega_{2c}|^2$. Thus the atomic susceptibilities corresponding to the two signal fields are given by

$$\chi_{1s} = \frac{2N|\wp_{ba}|^2}{\hbar\varepsilon_0V}\frac{\rho_{ab}}{\Omega_{1s}} = \frac{N|\wp_{ba}|^2}{\hbar\varepsilon_0V}\frac{4(\Delta - i\gamma)\Delta - |\Omega_{2c}|^2 + \Omega_{1c}\Omega_{2c}^*\Omega_{2s}/\Omega_{1s}}{(\Delta - i\gamma)(4\Delta^2 - |\Omega_c|^2 - i4\Delta\gamma)}, \quad (10a)$$

$$\chi_{2s} = \frac{2N|\wp_{bd}|^2}{\hbar\varepsilon_0V}\frac{\rho_{db}}{\Omega_{2s}} = \frac{N|\wp_{bd}|^2}{\hbar\varepsilon_0V}\frac{4(\Delta - i\gamma)\Delta - |\Omega_{1c}|^2 + \Omega_{1c}^*\Omega_{2c}\Omega_{1s}/\Omega_{2s}}{(\Delta - i\gamma)(4\Delta^2 - |\Omega_c|^2 - i4\Delta\gamma)}. \quad (10b)$$

The atomic susceptibilities above, relying on the four fields, indicate the process of four-wave mixing. But when the condition

$$\frac{\Omega_{1s}}{\Omega_{2s}} = \frac{\Omega_{1c}}{\Omega_{2c}} \quad (11)$$

is satisfied, equations (10) are reduced to

$$\chi_{1s} = \frac{N|\wp_{ba}|^2}{\hbar\varepsilon_0V}\frac{\Delta}{\Delta^2 - |\Omega_c|^2/4 - i\gamma\Delta}, \quad (12a)$$

$$\chi_{2s} = \frac{N|\wp_{bd}|^2}{\hbar\varepsilon_0V}\frac{\Delta}{\Delta^2 - |\Omega_c|^2/4 - i\gamma\Delta}. \quad (12b)$$

In the full resonance $\Delta = 0$, the two susceptibilities are null and the medium becomes completely transparent to

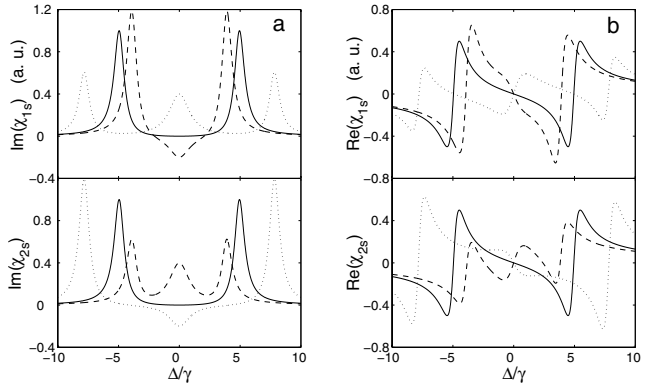

Fig. 2. Atomic susceptibilities as functions of the normalized detuning Δ/γ for detuning scheme I. The parameters are $\delta = 0$, $|\Omega_{1c}|/\gamma = 7$ and $|\Omega_{1s}|^2 = |\Omega_{2s}|^2$. Solid, dotted and dashed lines refer to the intensity ratios of the two control fields $|\Omega_{2c}|^2/|\Omega_{1c}|^2 = 1$, 4 and 0.25, respectively.

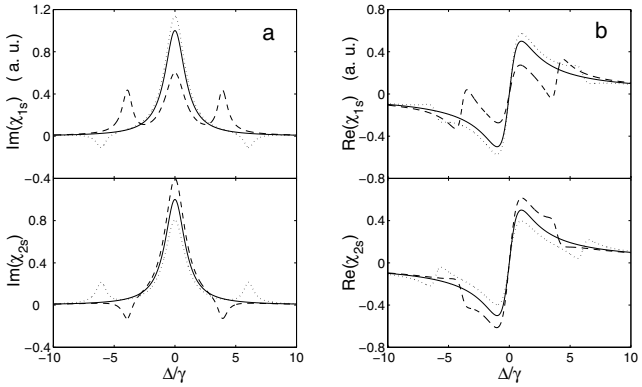

Fig. 3. Same as Figure 2 except $\delta = \pi$.

both signal fields. The results are the same as that for the EIT effect in a three-level atomic system [1,23]. The coexistence of EIT for the two signal fields implies the correlation between the two Λ channels. Therefore, equation (11) is the condition of the correlated EIT effect occurring in the double-Λ configuration. However, condition (11) indicates a phase matching relation

$$\delta \equiv \arg[\Omega_{1c}] - \arg[\Omega_{2c}] + \arg[\Omega_{2s}] - \arg[\Omega_{1s}] = 0. \quad (13)$$

Figure 2 shows the atomic susceptibilities as functions of the normalized detuning for detuning scheme I, where the parameters $\delta = 0$, $|\Omega_{1c}/\gamma| = 7$ and $|\Omega_{1s}|^2 = |\Omega_{2s}|^2$. Similar to a three-level EIT system, the two main absorption peaks in the imaginary part are located at $\Delta = \pm(1/2)|\Omega_c|$. For $|\Omega_{1c}|^2 = |\Omega_{2c}|^2$ (solid lines in Fig. 2) condition (11) is satisfied, and the two susceptibilities χ_{1s} and χ_{2s} are identical and null around $\Delta = 0$, which displays the correlated EIT effect. Otherwise, the dips/peaks of the imaginary susceptibilities at $\Delta = 0$ indicate the gain/loss for the signal fields. For example, when $|\Omega_{2c}|^2/|\Omega_{1c}|^2 = 4$ (dotted lines in Fig. 2), signal Ω_{2s} gets a gain while signal Ω_{1s} gets a loss. In result, Ω_{2s} increases and Ω_{1s} decreases until condition (11) is satisfied. Correspondingly, the real susceptibility for field Ω_{2s} (Ω_{1s}) exhibits a normal (abnormal) dispersion.

Now we propose an opposite effect to the correlated EIT in the double-Λ configuration, named as the correlated two-signal absorption (CTSA). When the four fields satisfy the condition

$$\frac{\Omega_{1s}}{\Omega_{2s}} = -\frac{\Omega_{2c}^*}{\Omega_{1c}^*}, \quad (14)$$

equations (10) can be reduced to

$$\chi_{1s} = \frac{N|\wp_{ba}|^2}{\hbar\varepsilon_0 V}\frac{1}{\Delta - i\gamma}, \quad (15a)$$

$$\chi_{2s} = \frac{N|\wp_{bd}|^2}{\hbar\varepsilon_0 V}\frac{1}{\Delta - i\gamma}, \quad (15b)$$

which correspond to the susceptibilities of two two-level subsystems. This implies the quantum coherence of the two lower levels is completely released. We note that the CTSA condition (14) denotes a phase matching parameter $\delta = \pi$.

Figure 3 shows the susceptibilities curves for the phase matching $\delta = \pi$, and other parameters are the same as in Figure 2. Here we can see that the absorption peaks appear at the resonance. For $|\Omega_{1c}|^2 = |\Omega_{2c}|^2$ (solid lines in Fig. 3), the CTSA condition (14) is satisfied, and the two susceptibilities χ_{1s} and χ_{2s} are identical to that of two-level atom. Though the Raman transition exists in each Λ channel, EIT disappears completely due to the decoupling between the two Λ channels. However, when the phase matching $\delta = \pi$, but the CTSA condition is not satisfied (both dotted and dashed lines in Fig. 3), the absorption of both signal fields occurs, too.

Similarly, in detuning scheme II, the stationary equations are approximately written as

$$\gamma\rho_{ab} = (i/2)(\Omega_{1s} + \Omega_{1c}\rho_{cb}), \quad (16a)$$

$$(\gamma + i\Delta)\rho_{db} = (i/2)(\Omega_{2s} + \Omega_{2c}\rho_{cb}), \quad (16b)$$

$$0 = \Omega_{1c}^*\rho_{ab} + \Omega_{2c}^*\rho_{db}, \quad (16c)$$

and the atomic susceptibilities are obtained to be

$$\chi_{1s} = \frac{N|\wp_{ba}|^2}{\hbar\varepsilon_0 V}\frac{|\Omega_{2c}|^2 - \Omega_{1c}\Omega_{2c}^*\Omega_{2s}/\Omega_{1s}}{\Delta|\Omega_{1c}|^2 - i\gamma|\Omega_c|^2}, \quad (17a)$$

$$\chi_{2s} = \frac{N|\wp_{bd}|^2}{\hbar\varepsilon_0 V}\frac{|\Omega_{1c}|^2 - \Omega_{1c}^*\Omega_{2c}\Omega_{1s}/\Omega_{2s}}{\Delta|\Omega_{1c}|^2 - i\gamma|\Omega_c|^2}. \quad (17b)$$

We see again that equation (11) is the condition for the correlated EIT effect under which the two susceptibilities are null, $\chi_{1s} \equiv \chi_{2s} \equiv 0$, thus irrelevant to the detuning. This is due to the fact that the Raman resonant transition exists in both Λ channels. However, when the CTSA condition (14) is satisfied, equation (17) is written as

$$\chi_{1s} = \frac{N|\wp_{ba}|^2}{\hbar\varepsilon_0 V}\frac{1}{\Delta|\Omega_{1c}|^2/|\Omega_c|^2 - i\gamma}, \quad (18a)$$

$$\chi_{2s} = \frac{N|\wp_{bd}|^2}{\hbar\varepsilon_0 V}\frac{1}{\Delta|\Omega_{1c}|^2/|\Omega_c|^2 - i\gamma}. \quad (18b)$$

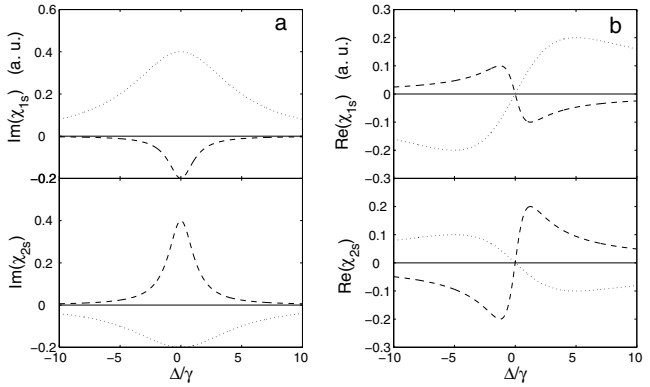

Fig. 4. Atomic susceptibilities as functions of the normalized detuning Δ/γ for detuning scheme II. The parameters are $\delta = 0$ and $|\Omega_{1s}|^2 = |\Omega_{2s}|^2$. Solid, dotted and dashed lines refer to the intensity ratios of the two control fields $|\Omega_{2c}|^2 / |\Omega_{1c}|^2 = 1$, 4 and 0.25, respectively.

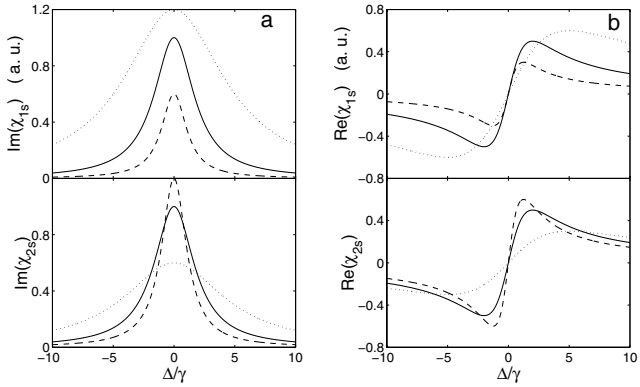

Fig. 5. Same as Figure 4 except $\delta = \pi$.

Similar to equation (15), equation (18) reflects the susceptibilities of two-level subsystems. Though the detuning exists in one Λ channel, it equally affects both susceptibilities due to the correlation between two Λ channels.

For detuning scheme II, we plot the susceptibilities as functions of the normalized detuning in Figures 4 and 5 for the phase matching $\delta = 0$ and π, respectively, where $|\Omega_{1s}|^2 = |\Omega_{2s}|^2$. The variation of the susceptibilities around $\Delta = 0$ is similar to that of detuning scheme I (see Figs. 2 and 3). In Figure 4, the solid lines show null susceptibilities all over the detuning range for $|\Omega_{1c}|^2 = |\Omega_{2c}|^2$, since the EIT condition (11) is satisfied.

To understand both the correlated EIT and CTSA effects, we consider the interaction Hamiltonian for a single atom

$$H_I = -\frac{\hbar}{2}(\Omega_{1s}\,|a\rangle\langle b| + \Omega_{2s}\,|d\rangle\langle b| + \Omega_{1c}\,|a\rangle\langle c| + \Omega_{2c}\,|d\rangle\langle c| + H.c.), \quad (18)$$

and formulate its eigenstates. Under condition (11), the dark state for the null eigenvalue is given by

$$|D\rangle = \frac{\Omega_{1c}\,|b\rangle - \Omega_{1s}\,|c\rangle}{\sqrt{|\Omega_{1c}|^2 + |\Omega_{1s}|^2}} = \frac{\Omega_{2c}\,|b\rangle - \Omega_{2s}\,|c\rangle}{\sqrt{|\Omega_{2c}|^2 + |\Omega_{2s}|^2}}. \quad (19)$$

Since two Λ channels share a common dark state, the EIT for the two signal fields are correlated. Contrarily, the dark state is not the eigenstate of the system under condition (14). Instead, the four eigenstates of the Hamiltonian are obtained as

$$|\Psi_{1,2}\rangle = \frac{1}{\sqrt{2}}\left(\frac{\Omega_{1s}\,|a\rangle + \Omega_{2s}\,|d\rangle}{\sqrt{|\Omega_{1s}|^2 + |\Omega_{2s}|^2}} \pm |b\rangle\right), \quad \text{for eigenvalues} \pm\sqrt{|\Omega_{1s}|^2 + |\Omega_{2s}|^2}, \quad (20a)$$

$$|\Psi_{3,4}\rangle = \frac{1}{\sqrt{2}}\left(\frac{\Omega_{1c}\,|a\rangle + \Omega_{2c}\,|d\rangle}{\sqrt{|\Omega_{1c}|^2 + |\Omega_{2c}|^2}} \pm |c\rangle\right), \quad \text{for eigenvalues} \pm\sqrt{|\Omega_{1c}|^2 + |\Omega_{2c}|^2}. \quad (20b)$$

In these states, there is no quantum coherence between the two lower levels. With the atomic decay of the upper levels taken into account, the eigenstates are unstable. In the next section, we will see that condition (14) refers to decay wave.

4 Analytical solutions of the propagation equations of the signal fields

In the following, we focus on the resonant case ($\Delta = 0$) and the two schemes have no difference. Using the same approximation as indicated above, we perform Fourier transforms to the atomic variables and the two signal fields, and obtain

$$(\gamma - i\omega)\tilde{\rho}_{ab}(z,\omega) = (i/2)[\widetilde{\Omega}_{1s}(z,\omega) + \Omega_{1c}\tilde{\rho}_{cb}(z,\omega)], \quad (21a)$$

$$(\gamma - i\omega)\tilde{\rho}_{db}(z,\omega) = (i/2)[\widetilde{\Omega}_{2s}(z,\omega) + \Omega_{2c}\tilde{\rho}_{cb}(z,\omega)], \quad (21b)$$

$$-\omega\tilde{\rho}_{cb}(z,\omega) = (1/2)[\Omega^*_{1c}\tilde{\rho}_{ab}(z,\omega) + \Omega^*_{2c}\tilde{\rho}_{db}(z,\omega)], \quad (21c)$$

$$c\frac{\partial\widetilde{\Omega}_{1s}(z,\omega)}{\partial z} - i\omega\widetilde{\Omega}_{1s}(z,\omega) = \frac{i}{2}g^2N\tilde{\rho}_{ab}(z,\omega), \quad (22a)$$

$$c\frac{\partial\widetilde{\Omega}_{2s}(z,\omega)}{\partial z} - i\omega\widetilde{\Omega}_{2s}(z,\omega) = \frac{i}{2}g^2N\tilde{\rho}_{db}(z,\omega), \quad (22b)$$

where $\widetilde{\Omega}_{1s}(z,\omega)$, $\widetilde{\Omega}_{2s}(z,\omega)$ and $\tilde{\rho}(z,\omega)$ are the Fourier transforms of $\Omega_{1s}(z,t)$, $\Omega_{2s}(z,t)$ and $\rho(z,t)$, respectively. Eliminating the atomic variables, we arrive at

$$\frac{\partial\widetilde{\Omega}_{1s}}{\partial z} = i\left[\frac{\omega}{c} - f\frac{|\Omega_{2c}|^2 - 4(\omega+i\gamma)\omega}{(\omega+i\gamma)(|\Omega_c|^2 - 4\omega^2 - 4i\gamma\omega)}\right]\widetilde{\Omega}_{1s} + if\frac{\Omega^*_{2c}\Omega_{1c}}{(\omega+i\gamma)(|\Omega_c|^2 - 4\omega^2 - 4i\gamma\omega)}\widetilde{\Omega}_{2s}, \quad (23a)$$

$$\frac{\partial\widetilde{\Omega}_{2s}}{\partial z} = i\left[\frac{\omega}{c} - f\frac{|\Omega_{1c}|^2 - 4(\omega+i\gamma)\omega}{(\omega+i\gamma)(|\Omega_c|^2 - 4\omega^2 - 4i\gamma\omega)}\right]\widetilde{\Omega}_{2s} + if\frac{\Omega^*_{1c}\Omega_{2c}}{(\omega+i\gamma)(|\Omega_c|^2 - 4\omega^2 - 4i\gamma\omega)}\widetilde{\Omega}_{1s}, \quad (23b)$$

where $f = g^2N/4c$. Equations (23) can be solved as

$$\widetilde{\Omega}_{1s}(z,\omega) = \frac{|\Omega_{1c}|^2\,\widetilde{\Omega}_{1s}(0,\omega) + \Omega_{1c}\Omega_{2c}^*\widetilde{\Omega}_{2s}(0,\omega)}{|\Omega_c|^2}e^{ik_+z} + \frac{|\Omega_{2c}|^2\,\widetilde{\Omega}_{1s}(0,\omega) - \Omega_{1c}\Omega_{2c}^*\widetilde{\Omega}_{2s}(0,\omega)}{|\Omega_c|^2}e^{ik_-z}, \tag{24a}$$

$$\widetilde{\Omega}_{2s}(z,\omega) = \frac{\Omega_{1c}^*\Omega_{2c}\widetilde{\Omega}_{1s}(0,\omega) + |\Omega_{2c}|^2\,\widetilde{\Omega}_{2s}(0,\omega)}{|\Omega_c|^2}e^{ik_+z} + \frac{-\Omega_{1c}^*\Omega_{2c}\widetilde{\Omega}_{1s}(0,\omega) + |\Omega_{1c}|^2\,\widetilde{\Omega}_{2s}(0,\omega)}{|\Omega_c|^2}e^{ik_-z}, \tag{24b}$$

where the two characteristic complex wavevectors are given by

$$k_+ = \frac{\omega}{c} + \frac{4f\omega}{|\Omega_c|^2 - 4(\omega+i\gamma)\omega}, \tag{25a}$$

$$k_- = \frac{\omega}{c} - \frac{f}{\omega+i\gamma}. \tag{25b}$$

Assuming the two signal fields have so slowly varying envelopes that $\omega \ll \gamma$, we can expand equations (25) as

$$k_+ = \omega/V_+ + O(\omega^2/\gamma^2), \tag{26a}$$

$$k_- = i(f/\gamma) + \omega/V_- + O(\omega^2/\gamma^2), \tag{26b}$$

where the group velocities $V_\pm$ are defined as

$$V_+ = \mathrm{Re}\left(\frac{d\omega}{dk_+}\right) = \frac{|\Omega_c|^2}{|\Omega_c|^2 + g^2N}c, \tag{27a}$$

$$V_- = \mathrm{Re}\left(\frac{d\omega}{dk_-}\right) = \frac{\gamma^2}{\gamma^2 - g^2N/4}c. \tag{27b}$$

The expression of the group velocity V_+ is the same as that of the three-level EIT system.

We neglect the high order terms in the complex wavevectors (26). The first term in wavevector k_- introduces the spatial decay of the signal fields. Consequently, the propagation of the signal field consists of two parts: the stationary waves $\widetilde{\Omega}_{is}^{(sw)}(z,\omega)$ $(i=1,2)$ (the first term in equations (24)) and the decay waves $\widetilde{\Omega}_{is}^{(dw)}(z,\omega)$ $(i=1,2)$ (the second term in equations (24)), corresponding to the wavevectors k_+ and k_-, respectively. From equation (24) we find that the stationary waves and the decay waves obey the EIT and CTSA conditions

$$\frac{\widetilde{\Omega}_{1s}^{(sw)}(z,\omega)}{\widetilde{\Omega}_{2s}^{(sw)}(z,\omega)} = \frac{\Omega_{1c}}{\Omega_{2c}}, \tag{28a}$$

$$\frac{\widetilde{\Omega}_{1s}^{(dw)}(z,\omega)}{\widetilde{\Omega}_{2s}^{(dw)}(z,\omega)} = -\frac{\Omega_{2c}^*}{\Omega_{1c}^*}, \tag{28b}$$

respectively. If the initial signal fields $\widetilde{\Omega}_{1s}(0,\omega)$ and $\widetilde{\Omega}_{2s}(0,\omega)$ satisfy the EIT condition (28a), the decay waves do not exist and the two signal fields are completely transparent in the medium, that is, $\widetilde{\Omega}_{1s}(z,\omega) = \widetilde{\Omega}_{1s}(0,\omega)\exp(ik_+z)$ and $\widetilde{\Omega}_{2s}(z,\omega) = \widetilde{\Omega}_{2s}(0,\omega)\exp(ik_+z)$. However, if the initial signal fields $\widetilde{\Omega}_{1s}(0,\omega)$ and $\widetilde{\Omega}_{2s}(0,\omega)$ satisfy the CTSA condition (28b), the stationary waves do not occur and the solutions are $\widetilde{\Omega}_{1s}(z,\omega) = \widetilde{\Omega}_{1s}(0,\omega)\exp(ik_-z)$ and $\widetilde{\Omega}_{2s}(z,\omega) = \widetilde{\Omega}_{2s}(0,\omega)\exp(ik_-z)$, which decay and disappear in propagation.

Now we focus on the stationary waves and define the amplification ratios for them

$$n_{1s} \equiv \frac{\left|\widetilde{\Omega}_{1s}^{(sw)}(z,\omega)\right|^2}{\left|\widetilde{\Omega}_{1s}(0,\omega)\right|^2} = \frac{1+\xi\mu_0+2\sqrt{\xi\mu_0}\cos(\delta_0)}{(1+\xi)^2}, \tag{29a}$$

$$n_{2s} \equiv \frac{\left|\widetilde{\Omega}_{2s}^{(sw)}(z,\omega)\right|^2}{\left|\widetilde{\Omega}_{2s}(0,\omega)\right|^2} = \frac{\xi^2+\xi/\mu_0+2\xi\sqrt{\xi/\mu_0}\cos(\delta_0)}{(1+\xi)^2}, \tag{29b}$$

where the intensity ratio between the two initial signals and the intensity ratio between the two control fields are designated by $\mu_0 \equiv \left|\widetilde{\Omega}_{2s}(0,\omega)\right|^2 / \left|\widetilde{\Omega}_{1s}(0,\omega)\right|^2$ and $\xi \equiv |\Omega_{2c}|^2 / |\Omega_{1c}|^2$, respectively. The phase matching δ_0 for the initial fields is given by

$$\delta_0 \equiv \arg[\Omega_{1c}] - \arg[\Omega_{2c}] + \arg[\widetilde{\Omega}_{2s}(0,\omega)] - \arg[\widetilde{\Omega}_{1s}(0,\omega)]. \tag{30}$$

In the cases of $\delta_0 = 0$ and π, equation (29) is reduced to

$$n_{1s} = \frac{(1 \pm \sqrt{\xi\mu_0})^2}{(1+\xi)^2}, \tag{31a}$$

$$n_{2s} = \frac{(\xi \pm \sqrt{\xi/\mu_0})^2}{(1+\xi)^2} = \frac{\xi}{\mu_0}n_{1s}, \tag{31b}$$

where the plus and minus signs correspond to $\delta_0 = 0$ and π, respectively.

Figure 6 shows the amplification ratios of the signal fields as functions of μ_0 and ξ. In Figures 6a and 6b, where $\delta_0 = 0$, the thick solid lines, i.e. $\xi = \mu_0$, refer to the EIT condition and divide the surfaces into the amplification and attenuation parts. On the thick solid lines, however, we obtain $n_{1s} = n_{2s} = 1$. Correspondingly, in Figures 6c and 6d, where $\delta_0 = \pi$, the thick solid lines, i.e. $\xi\mu_0 = 1$, refer to the CTSA condition, and exhibit null signal fields $n_{1s} = n_{2s} = 0$.

The most important feature in the double-Λ atomic system is that the two stationary signal waves must satisfy EIT condition (28a), and this results in the shape-matched propagation of two signals.

5 Numerical simulation

We solve numerically a set of both the ordinary and partial differential equations (4, 5) and (7) at the resonant case

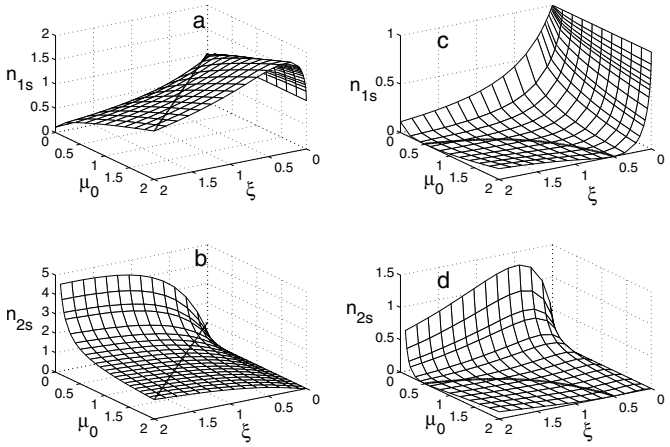

Fig. 6. Amplification ratios of the signal fields as functions of μ_0 and ξ, with the phase matching parameter $\delta_0 = 0$ and π in (a, b) and (c, d), respectively. The thick solid lines in (a, b) and (c, d) correspond to the EIT and CTSA conditions, respectively.

$\Delta = 0$. In the numerical simulation, we assume that all the atoms are initially at the ground state $|b\rangle$ and the two signal pulses are set to be the Gaussian type

$$\overline{\Omega}_{is}(\overline{z}, \tau = 0) = \overline{\Omega}_{is} \exp[-(\overline{z}/w_i)^2], \tag{32}$$

where $\overline{\Omega}_{is} = \Omega_{is}/(g\sqrt{N})$, $\overline{z} = z\gamma/c$ and $\tau = \gamma t$ are normalized variables and w_i is the normalized length of the Gaussian pulse. The two control fields are assumed to be plane-waves with the normalized amplitudes $\overline{\Omega}_{ic} = \Omega_{ic}/(g\sqrt{N})$.

5.1 Set-up of shape-matched propagation

In Section 4, the analytical solution shows that there are two characteristic waves, the stationary and decay wave, satisfying the EIT condition (11) and the CTSA condition (14), respectively. The phase matching of the four fields dominates the occurrence of EIT and CTSA effects.

Figure 7 shows the CTSA effect when the initial four fields, $\overline{\Omega}_{1s} = 0.06$, $\overline{\Omega}_{2s} = -0.05$, $\overline{\Omega}_{1c} = 10$, $\overline{\Omega}_{2c} = 12$ ($\delta_0 = \pi$), satisfy the CTSA condition (14). The two signal pulses quench simultaneously after $\tau = 2$. In order to avoid signal absorption, we take the initial phase matching $\delta_0 = 0$ in the following simulation.

The main feature of the double-Λ configuration is the set-up of shape-matched propagation of two signal beams. This feature comes from the stationary-wave condition (28a) in the transmission: the modulation between two signal fields should be shape-matched as long as the ratio between the two control fields is constant. In Figure 8a, the two initial signal pulses have different shapes, i.e. $\overline{\Omega}_{1s} = 0.1, w_1 = 5$ and $\overline{\Omega}_{2s} = 0.05, w_2 = 10$, and are distant with $\Delta\overline{z} = 3$. At $\tau = 10$ the two pulses become shape-matched in propagation as shown in Figures 8b and 8c, where the control fields satisfy $\overline{\Omega}_{1c}/\overline{\Omega}_{2c} = 2$ and $\overline{\Omega}_{1c}/\overline{\Omega}_{2c} = 1$, respectively. Obviously, the amplitude ratio of two shape-matched pulses is equal to the amplitude ratio of two control fields. In Figure 8c, the two pulses become identical due to $\overline{\Omega}_{1c}/\overline{\Omega}_{2c} = 1$.

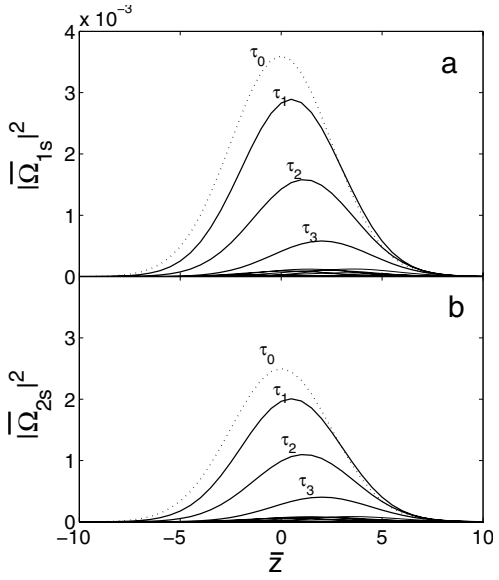

Fig. 7. Two signal pulses quench simultaneously when the initial four fields, $\overline{\Omega}_{1s} = 0.06$, $\overline{\Omega}_{2s} = -0.05$, $\overline{\Omega}_{1c} = 10$, $\overline{\Omega}_{2c} = 12$ ($\delta_0 = \pi$), satisfy the CTSA condition. Dotted lines show the initial pulses at τ_0 and solid lines show the evolution of the pulses for the time interval $\Delta\tau = 0.5$. In Figures 7–10, the coupling strength is $g\sqrt{N}/\gamma = 2.0$.

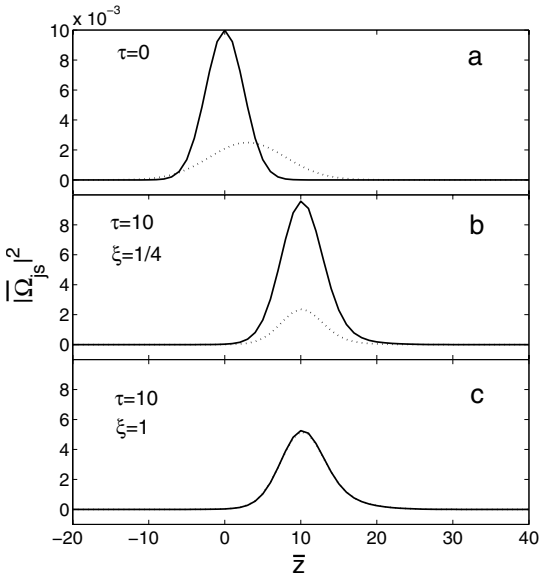

Fig. 8. Shape-matched propagation of two signal pulses where solid and dotted lines indicate signal beam 1 and 2, respectively. (a) At $\tau = 0$, the two initial pulses are $\overline{\Omega}_{1s} = 0.1, w_1 = 5$ and $\overline{\Omega}_{2s} = 0.05, w_2 = 10$. The two pulses at $\tau = 10$ for (b) $\overline{\Omega}_{1c}/\overline{\Omega}_{2c} = 2$ ($\xi = 1/4$) and (c) $\overline{\Omega}_{1c}/\overline{\Omega}_{2c} = 1$ ($\xi = 1$).

This feature can be further utilized in copying a signal from one beam to the other which may have different carrier frequency and/or polarization. In Figure 9, when one signal beam $\overline{\Omega}_{1s}(\overline{z}, 0)$, described by the dotted line, is injected into the medium, the twin signals are then

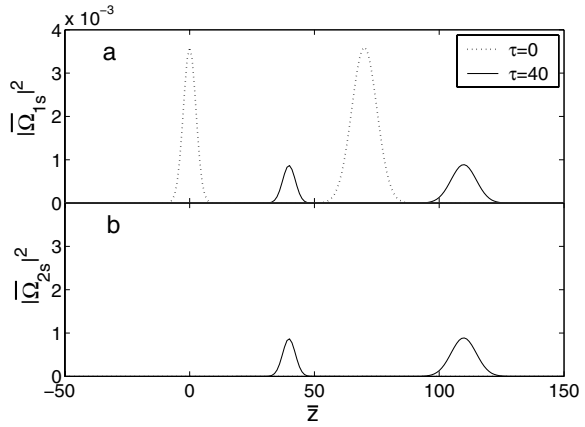

Fig. 9. Copy a signal from one beam to the other with equal control fields $\overline{\Omega}_{1c} = \overline{\Omega}_{2c} = 12$. Input signal with two pulses (dotted line) is described as $\overline{\Omega}_{1s}(\overline{z}, 0) = 0.06\exp[-(\overline{z}/5)^2] + 0.06\exp[-((\overline{z} - 70)/10)^2]$. Twin signals (solid lines) are obtained at $\tau = 40$.

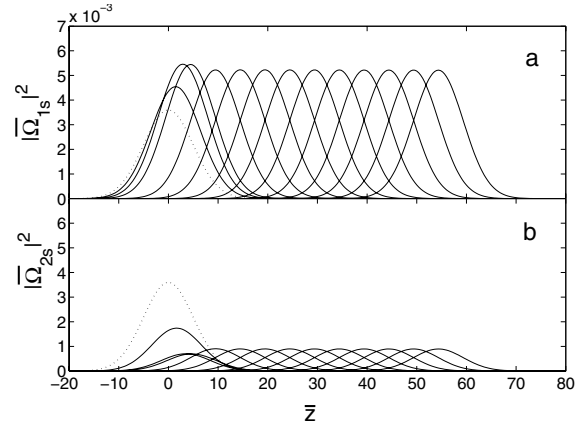

Fig. 10. Amplification of one signal in transmission. Dotted lines specify the two identical signals at $\tau = 0$. In propagation, the temporal interval for the first four lines is $\Delta\tau = 1.5$, and the interval of the other lines is $\Delta\tau = 5$.

generated with balanced control fields. However, the copy brings about attenuation of the original signal. According to equation (29), the maximal signal conversion efficiency is 25% [20].

In Section 4 we have discussed the amplification of input signal. In order to get perfect fidelity in signal amplification, we should input two shape-matched signals. If two signals are initially identical, i.e. $\mu_0 = 1$, the amplification ratios n_{1s} and n_{2s}, according to equation (31), reach the maximum 1.457 for $\xi = 3 - 2\sqrt{2}$ and $3 + 2\sqrt{2}$, respectively. Figure 10 shows the signal amplification of one input pulse against the attenuation of the other.

5.2 Controllable shape-matched propagation and transfer

In the double-Λ configuration, when the shape-matched propagation is set up, the signal transfer can occur not only between the fields and the atomic ensemble but also

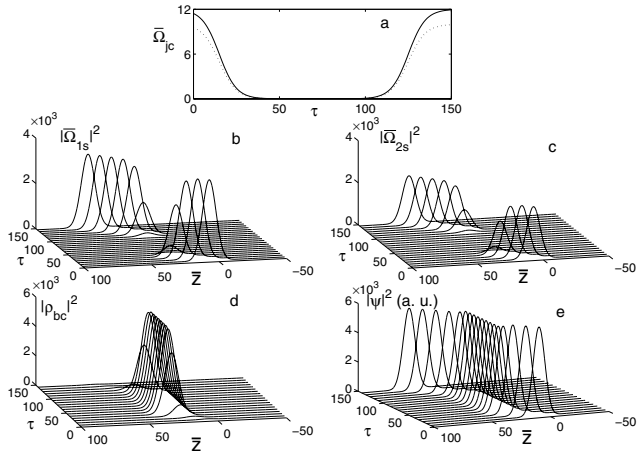

Fig. 11. Storing and retrieving process of two synchronous pulses in the double-Λ configuration. (a) Synchronous variation of two control fields, $\overline{\Omega}_{1c}$ (solid line) and $\overline{\Omega}_{2c}$ (dotted line); (b) and (c) propagation of two signal pulses $\left|\overline{\Omega}_{1s}\right|^2$ and $\left|\overline{\Omega}_{2s}\right|^2$, respectively; (d) evolution of the atomic coherence $|\rho_{bc}|^2$; (e) propagation of the dark state polariton-wave $|\psi|^2$. Peak values of the two input pulses are $\overline{\Omega}_{1s} = 0.06$ and $\overline{\Omega}_{2s} = 0.05$, and the maximum amplitudes of the two control fields, $\beta_{1c} = 12$ and $\beta_{2c} = 10$. In Figures 11–14, the coupling strength is $g\sqrt{N}/\gamma = 3.5$.

between the two signal fields. In this system, the dark state polariton is described by [17,19,26]

$$\psi = (\overline{\Omega}_{1s}\cos\phi + \overline{\Omega}_{2s}\sin\phi)\cos\theta - \rho_{bc}\sin\theta, \qquad (33)$$

where $\tan\theta = g\sqrt{N}/|\Omega_c|$ and $\tan\phi = \Omega_{2c}/\Omega_{1c}$. Obviously, the polariton-wave is the same as that in the three-level configuration, if the signal superposition $(\overline{\Omega}_{1s}\cos\phi + \overline{\Omega}_{2s}\sin\phi)$ is considered as a whole. The polariton-wave ψ propagates losslessly in the medium with a group velocity $V_+ = \frac{|\Omega_c|^2}{|\Omega_c|^2 + g^2 N}c = c\cos^2\theta$ (see Eq. (27a)). Here θ governs the signal transfer between fields and atomic medium, while ϕ governs the transfer between the two signal fields.

In Figure 11, we show the process of simultaneously storing and retrieving two signal fields by fixing ϕ. Figure 11a exhibits the synchronous variation of the two control fields given by

$$\overline{\Omega}_{ic}(\tau) = \beta_{ic}\{1 - 0.5\tanh[0.1(\tau - 15)] + 0.5\tanh[0.1(\tau - 125)]\}, \qquad (i = 1, 2) \quad (34)$$

where $\beta_{1c} = 12$ and $\beta_{2c} = 10$ are normalized amplitudes of the two control beams. The two input pulses are set to be shape-matched with $\overline{\Omega}_{1s} = 0.06$ and $\overline{\Omega}_{2s} = 0.05$, and the EIT condition (11) is initially satisfied. As is indicated above, the decay wave does not exist so that the input signals enter the medium without decaying. Figures 11b and 11c show that the two signal beams can be stored and retrieved simultaneously. However, the two signals are stored in the atomic coherence ρ_{bc} shown in Figure 11d, and the polariton-wave ψ in Figure 11e mostly maintains its magnitude in propagation.

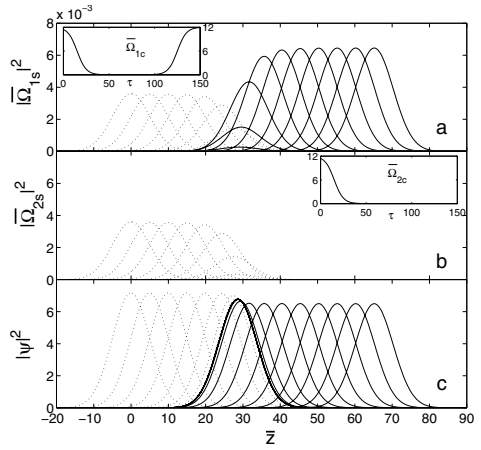

Fig. 12. Two identical signals are transferred into one field after the storage; (a) and (b) evolution of signal beam 1 and 2, respectively, where insets show variation of the control fields; (c) evolution of polariton-wave. Dotted and solid lines represent signal propagation processes before and after the storage, respectively. Time interval between adjacent lines is $\Delta\tau = 5$.

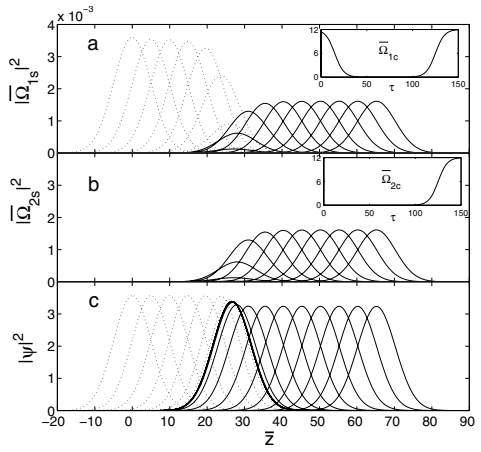

Fig. 13. One signal is divided into twin signals after the storage. Description is the same as in Figure 12.

According to equation (33), the cooperative variation of the parameters θ and ϕ may create a variety of schemes of signal transfer and storage, as shown in Figures 12–15. In Figure 12, the two control fields are identical ($\tan\phi = 1$) before the storage, and then the second control field vanishes ($\tan\phi = 0$) after the storage. The two identical signals written in the medium are transferred into one field in the reading stage, and hence the intensity of the retrieved signal is approximately doubled. Figure 13 exhibits an opposite process to Figure 12, and the twin signals are generated after the storage. However, in Figure 14, we show the signal transfer from one field to the other after the storage by adiabatically changing the two control fields. The signal conversion efficiency is nearly 100%. The signal transfer can also occur between the two signal fields without participation of atomic storage. In Figure 15, when the control field $\overline{\Omega}_{1c}$ is constant and the control field $\overline{\Omega}_{2c}$ varies similar to equation (34), the pulse transfers between the two signal fields. This effect is particularly interesting since, in the evolution $\theta \cong 0$, the atomic coherence of the two lower levels is not involved. This means that, in the double-Λ configuration, the EIT can build up the quantum coherence between two fields. In all these schemes, the polariton-waves propagate without significant decaying.

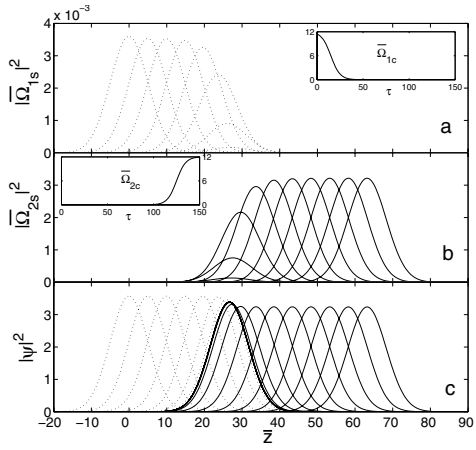

Fig. 14. Signal transfer from one field to the other after the storage. Description is the same as in Figure 12.

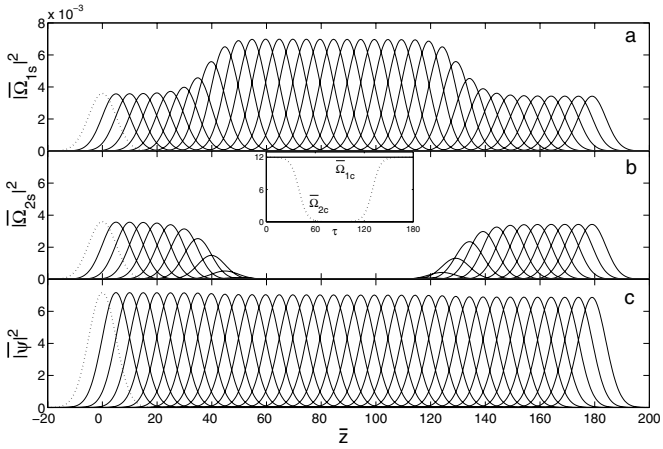

Fig. 15. Signal transfer between two fields without atomic storage process. Description is the same as in Figure 12.

6 Conclusion

In summary, we study in detail the atomic susceptibilities in the double-Λ configuration related to the phase matching of the four fields. Though quantum coherence occurs in each Λ channel, the EIT effect is also affected by the coherence between the two Λ channels. The phase matching of the four fields, $\delta = 0$ and $\delta = \pi$, dominates the constructive and destructive coherence, respectively. The former corresponds to a correlated EIT effect, in which two transmitted signal beams are shape-matched. In the latter case, however, the EIT coherence is released and the atomic susceptibilities behave as two two-level systems. The analytical results show that the general solution of the propagation equations consists of two characteristic

waves: the stationary and decay wave, associated with the EIT and CTSA effect, respectively. However, the EIT and CTSA conditions can be obtained by both the discussions of the atomic susceptibilities and the analysis of the propagation equations. The proportion of the input signals entering the medium can be controlled according to these conditions. In the numerical simulation, we show that in the double-Λ configuration the signal transfer can occur not only between the fields and the atoms but also between the two fields. Moreover, the conversion efficiency between the two signals can reach nearly 100%. Therefore, various schemes of manipulating optical synchronous signals have been shown and thus provide extensive application opportunities in quantum information technology.

This research was supported by the National Fundamental Research Program of China Project No. 2001CB309310, and the National Natural Science Foundation of China, Project No. 60278021 and No. 10574015. The one of the authors, K. Wang, acknowledges the financial support of the Abdus Salam International Centre for Theoretical Physics (ICTP) under the Associate Programm.

References

1. K.-J. Boller, A. Imamoglu, S.E. Harris, Phys. Rev. Lett. **66**, 2593 (1991); S.E. Harris, Phys. Rev. Lett. **70**, 552 (1993); S.E. Harris, Phys. Rev. Lett. **72**, 52 (1994); S.E. Harris, Phys. Today **50**, 36 (1997)
2. C. Liu, Z. Dutton, C.H. Behroozi, L.V. Hau, Nature **409**, 490 (2001)
3. D.F. Phillips, A. Fleischhauer, A. Mair, R.L. Walsworth, M.D. Lukin, Phys. Rev. Lett. **86**, 783 (2001)
4. M. Fleischhauer, M.D. Lukin, Phys. Rev. Lett. **84**, 5094 (2000)
5. M.D. Lukin, S.F. Yelin, M. Fleischhauer, Phys. Rev. Lett. **84**, 4232 (2000)
6. A.E. Kozhekin, K. Mølmer, E. Polzik, Phys. Rev. A **62**, 033809 (2000)
7. A.B. Matsko, Y.V. Rostovtsev, O. Kocharovskaya, A.S. Zibrov, M.O. Scully, Phys. Rev. A **64**, 043809 (2001)
8. M. Fleischhauer, M.D. Lukin, Phys. Rev. A **65**, 022314 (2002)
9. K. Wang, Sh. Zhu, Eur. Phys. J. D **20**, 281 (2002)
10. E. Cerboneschi, E. Arimondo, Phys. Rev. A **52**, R1823 (1995); E. Cerboneschi, E. Arimondo, Phys. Rev. A **54**, 5400 (1996)
11. E.A. Korsunsky, N. Leinfellner, A. Huss, S. Baluschev, L. Windholz, Phys. Rev. A **59**, 2302 (1999)
12. E.A. Korsunsky, D.V. Kosachiov, Phys. Rev. A **60**, 4996 (1999)
13. A.J. Merriam, S.J. Sharpe, M. Shverdin, D. Manuszak, G.Y. Yin, S.E. Harris, Phys. Rev. Lett. **84**, 5308 (2000)
14. M.D. Lukin, P.R. Hemmer, M.O. Scully, Adv. At. Mol. Opt. Phys. **42**, 347 (2000)
15. M.G. Payne, L. Deng, Phys. Rev. A **65**, 063806 (2002)
16. L. Deng, M.G. Payne, Phys. Rev. Lett. **91**, 243902 (2003)
17. A. Raczynski, J. Zaremba, S. Zielinska-Kaniasty, Phys. Rev. A **69**, 043801 (2004)
18. Xiong-Jun Liu, Hui Jing, Xiao-Ting Zhou, Mo-Lin Ge, Phys. Rev. A **70**, 015603 (2004)
19. Xiong-Jun Liu, Hui Jing, Mo-Lin Ge, e-print `arXiv:quant-ph/0403171`
20. Ying Wu, Xiaoxue Yang, Phys. Rev. A **70**, 053818 (2004)
21. Zhuang Li, De-Zhong Cao, Kaige Wang, Phys. Lett. A **341**, 366 (2005)
22. Kaige Wang, Fanglin Peng, Guojian Yang, J. Opt. B: Quant. Semiclass. Opt. **5**, 44 (2003)
23. M.O. Scully, M.S. Zubairy, *Quantum Optics* (Cambrige University Press, 1997)
24. Y. Wu, J. Saldana, Y. Zhu, Phys. Rev. A **67**, 013811 (2003)
25. M. Jain, H. Xia, G.Y. Yin, A.J. Merriam, S.E. Harris, Phys. Rev. Lett. **77**, 4326 (1996)
26. Zhuang Li, Lisen Xu, Kaige Wang, Phys. Lett. A **346**, 269 (2005)